Chapter 4

Study on the Preparation of Solar Grade Silicon by Metallurgical Method

Dawei Luo

Additional information is available at the end of the chapter

http://dx.doi.org/10.5772/67643

Abstract

The global PV industry has rapidly developed over the past decade, which has led to a large demand for silicon materials. Solar cells are currently fabricated from a variety of silicon-based materials. However, current market is difficult to ensure a steady supply for this material. Development of a new process to produce silicon at low cost is definitely necessary. Metallurgical grade silicon (MG-Si) with the purity of 98%, which is produced by carbothermic reduction in electric arc furnaces, has been considered as a cheap starting material for conversion to purity of 99.99%. Many alternative methods for purifying MG-Si to Solar grade silicon (SoG-Si) have been explored, for example, (1) pyro metallurgical processes, (2) hydrometallurgical processes and (3) electrochemical methods. Metallurgical route is recognized as a promising process to meet market demand for solar energy silicon material, which is different from the traditional Siemens process. This chapter focuses on the introduction of three kinds of typical impurity removal methods in metallurgical process, and the impurity removal effect of different processes was analysed and discussed.

Keywords: metallurgical grade silicon, solar grade silicon, acid leaching, electron beam melting, electromagnetic induction slag melting

1. Introduction

The rapid development of photovoltaic industry results in lack of silicon feedstock which meets technical and economic requirements of the photovoltaic cells. More and more attentions have been paid to the research of producing solar grade silicon (SOG-Si) by refining metallurgical grade silicon. Metallurgical route is recognized as a promising process to meet market demand for solar energy silicon material, which is different from the traditional Siemens process. There are many ways to remove impurities in metallurgical process, this chapter focuses

on the three typical kinds of impurity removal process in detail, which is the process of acid leaching process, electron beam process and electromagnetic induction slagging process.

2. Purification of metallurgical grade silicon (MG-Si) by acid leaching

2.1. Characterization of MG-Si

Pre-treatment of metallurgical grade silicon (MG-Si) is an important part in metallurgical purification process because it can remove the metallic impurities such as aluminium, iron and calcium effectively under acid leaching process. Among above methods, hydrometallurgical method is recognized as the best pre-treatment process for silicon refining because metallic impurities can be removed from MG-Si by this process without large amounts of energy consumption and capital investment of equipment. A series of comparative experiments were designed to study the effect of acid leaching parameters on impurities removal efficiency in detail. The effects of acid agent, acid concentration, time, temperature and silicon particle size on impurities removal efficiency were investigated, respectively.

Impurities contents and their segregation coefficients in MG-Si are listed in **Table 1** [1]. The major metallic impurities are aluminium (0.271%), iron (0.234%) and calcium (0.058%).

Microstructures of MG-Si are shown in **Figure 1**. The bright phases at the grain boundaries are the segregation of metal impurities. The qualitative composition of bright phases and their relative content in MG-Si are listed in **Table 2**. It has been studied that the sensitivity of phases in the samples to hydrochloric acid and hydrofluoric acid, all of the phases in the samples can be removed by the hydrofluoric acid and hydrochloric acid but the Fe-Si and Fe-Ti-Si phases cannot be attacked by hydrochloric acid. According to the sensitivity of these phases to the

Element	Concentration ($mg \cdot kg^{-1}$)	Segregation coefficient
Al	2709	2.0×10^{-3}
Fe	2339	8×10^{-6}
Ca	575	8×10^{-3}
Ti	198	2×10^{-6}
Cu	27	4×10^{-4}
Mn	124	1.3×10^{-5}
Mg	21	3.2×10^{-6}
Zn	<2	1×10^{-5}
Cr	<2	1.45×10^{-5}
B	15	0.8
P	20	0.35

Table 1. Impurity contents and their segregation coefficients in MG-Si.

http://dx.doi.org/10.5772/67643

acids in **Table 2**, hydrochloric acid and hydrofluoric acid are selected as acid agents in this chapter. The removal efficiency of aluminium, iron and calcium after the acid leaching by hydrochloric acid and hydrofluoric acid are checked.

2.2. Effect of various acid leaching parameters on the impurity content

MG-Si was crushed by the crushing mill and grinded with the attritor which were composed of adamantine spar container and Al_2O_3-sintered hard ceramic balls before the leaching experiments. And then silicon particles were sieved to different particle sizes for leaching trials. Different particle sizes silicon were disposed by acetone solution under ultrasonic wave and washed by the deionized water. Leaching trials were done with aqueous thermostat after the silicon powders were dried. The mass of silicon powders employed at a time was 10 g and the liquid-solid weight ratio of 10:1. After each experiment, silicon powder was filtered and washed with deionized water. The contents of aluminium, iron and calcium under different acid leaching conditions were analysed by inductively coupled plasma atomic emission spectrometer (ICP-AES), respectively. A larger number of leaching trials were performed in a systematic way in order to study the effect of the acid agent, acid concentration, time, temperature

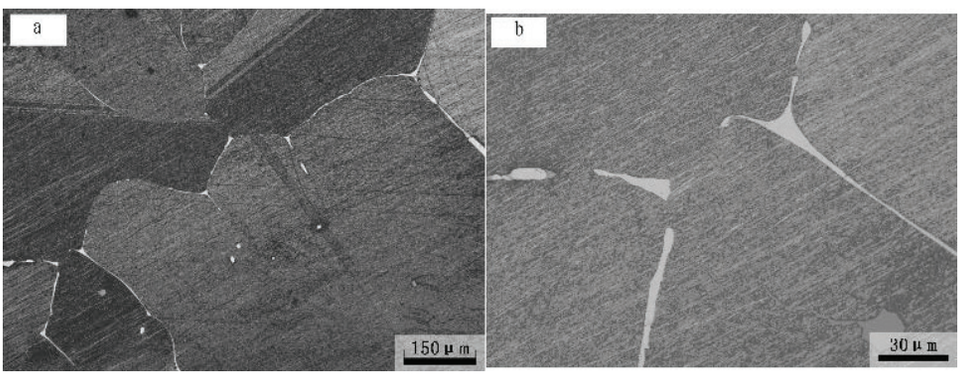

Figure 1. The metallographs of MG-Si: (a) the low power microstructure and (b) local amplification bright phases at the grain boundaries.

Composition of phases	Relative abundance	Sensitivity	
		Hydrochloric acid	Hydrofluoric acid
Si-Fe	***		*
Si-Fe -A1	***	*	*
Si-Fe-Ti	**		*
Si-Fe-A1-Ti	***	*	*
Si-Fe-A1-Ca	**	*	*
Si-Fe-A1-Ca-Ti	**	*	*
Si-Ca	*	*	*

Table 2. The main precipitated phases and their sensitivity for hydrochloric acid and hydrofluoric acid in MG-Si [2].

and silicon particle size on the removal efficiencies of impurities element. Specific results were described in the following sections in more detail.

2.2.1. Effect of acid agent and acid concentration on the impurity content

The change of impurity content as increasing the concentration of the hydrofluoric and hydrochloric acids was plotted in **Figure 2**. The content of aluminium and iron gradually decreased with the increasing concentration of hydrochloric acid but the change regularity of calcium content was in equable. Calcium content reduced first and then grew little with the increasing concentration of hydrochloric acid. The minimum value achieved at 15%. This was because the silicon powders generated passivation when the concentration of hydrochloric acid exceeded 15%. The change tendency for the content of aluminium, iron and calcium after the hydrofluoric acid treatment were very different. Aluminium content increased and iron content gradually decreased with the increasing concentration of hydrofluoric acid. Calcium content reduced first and then grew little, the minimum value was achieved at 2%. The reason for the unusual change regularity of aluminium and calcium was most probably due to the formation of insoluble fluorides.

2.2.2. Effect of acid temperature on the impurity content

The effect of temperatures on the impurity contents was demonstrated in **Figure 3**. The content change of aluminium, iron and calcium with temperatures was coincident after leaching with hydrochloric acid. They all gradually decreased with temperatures. But the results were diverse after leaching with hydrofluoric acid. As the increasing temperatures, the content of iron gradually decreased, but the contents of aluminium and calcium reduced first and then grew little. The minimum value was achieved at 40 and 60°C, respectively. The reason for above phenomenon was most probably due to the formation of insoluble fluorides.

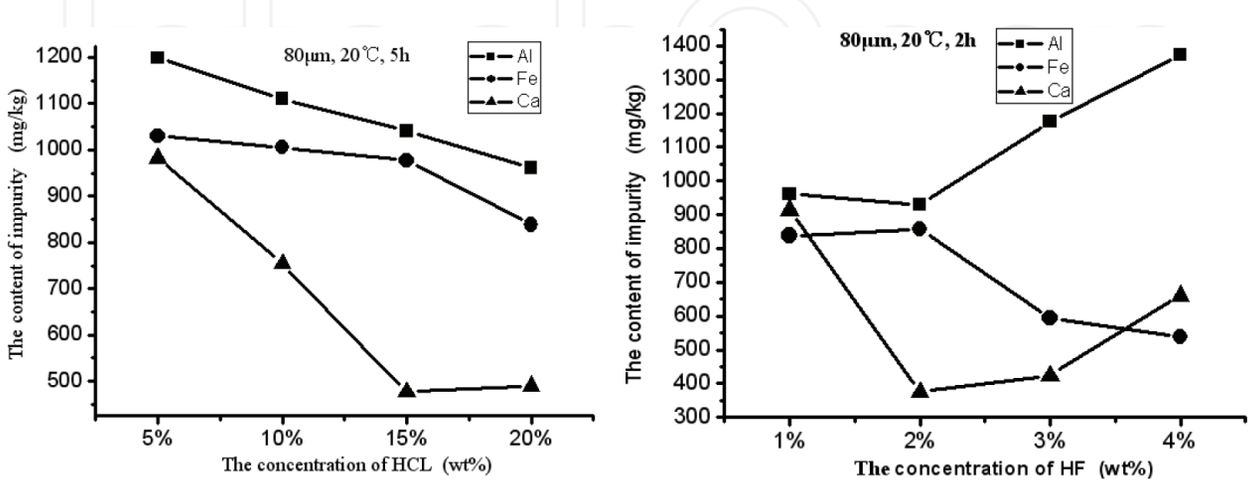

Figure 2. Final impurity content after leaching with hydrochloric acid and hydrofluoric acid at different concentrations.

http://dx.doi.org/10.5772/67643

2.2.3. Effect of acid time on the impurity content

The effect of the leaching times on the impurity contents is shown in **Figure 4**. The content change of aluminium, iron and calcium with the increasing leaching times was the same after leaching with hydrochloric acid. They all reduced first and then grew little; the minimum value was achieved at 10 h. The content change of iron and calcium with times after hydrofluoric acid leaching was the same as that after hydrochloric acid leaching. The minimum value achieved at 2 h. But the aluminium content gradually decreased with the increasing times.

2.2.4. Effect of particle sizes on the impurity content

The effect of the particle sizes on the impurity contents is demonstrated in **Figure 5**. The content change of aluminium, iron and calcium with particle sizes was alike after leaching with hydrochloric and hydrofluoric acids. The contents of aluminium, iron and calcium gradually depressed with the increasing particle sizes.

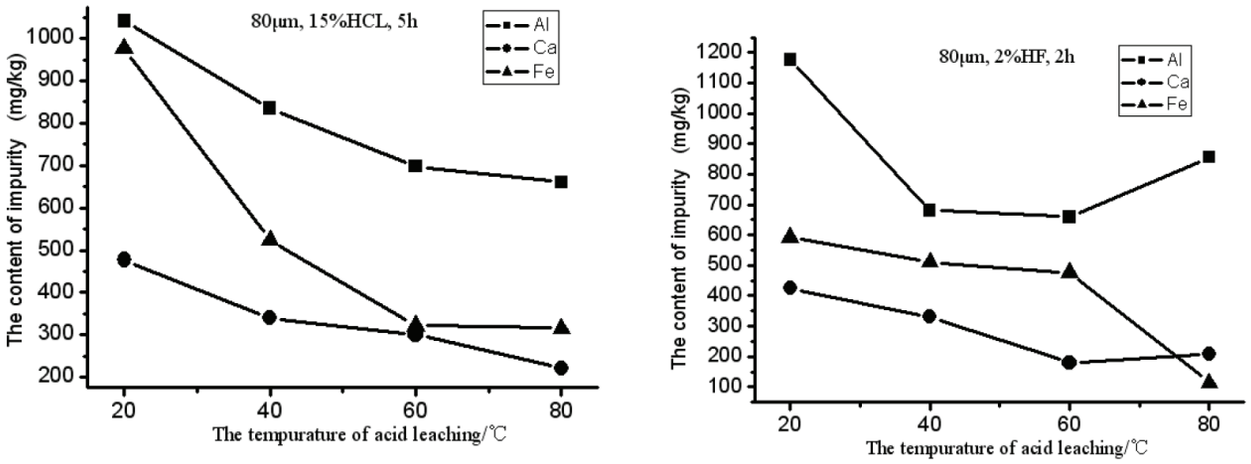

Figure 3. Final impurity content after leaching with hydrochloric acid land hydrofluoric acid at different temperatures.

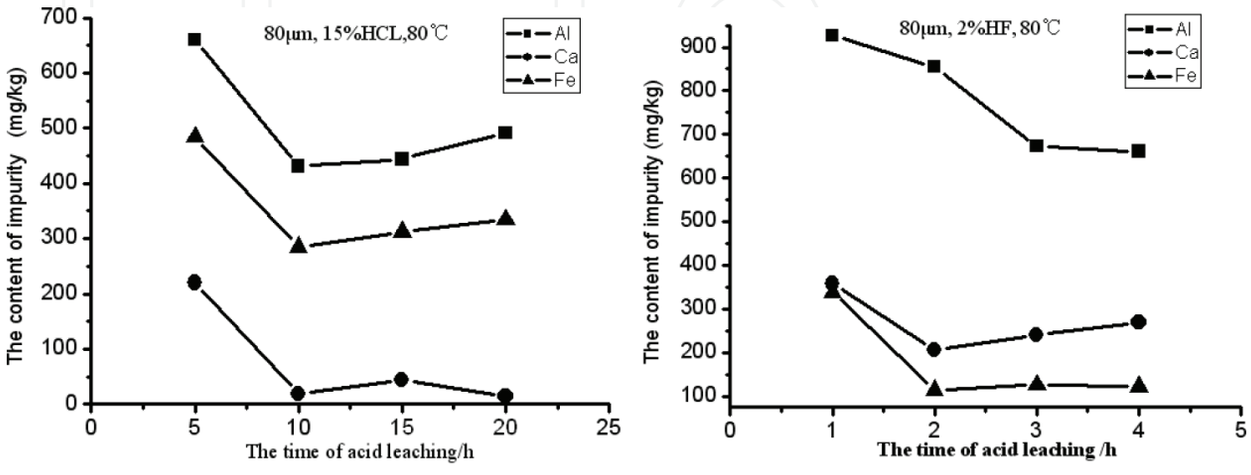

Figure 4. Final impurity content after leaching with hydrochloric acid and hydrofluoric acid at different leaching times.

The total content of aluminium, iron and calcium impurities reached minimum at 100 μm. This result was opposite to some previous research. In order to explain this consequence, the content of major impurities in MG-Si at different particle sizes was analysed by ICP-AES before acid leaching. The measurement result is illustrated in **Figure 6**. The content of major impurities in silicon particles with 30 μm was higher than that with 80 μm. It suggested that more friable phases that included more impurities were aggregated to the finer fraction during sieving. A similar grain size effect was found for other minor impurities. Impurities such as the doping elements boron and phosphorus with unfavourable segregation coefficients were not greatly affected by acid leaching. However, they must be removed by pyro metallurgical treatment or a similar method [3].

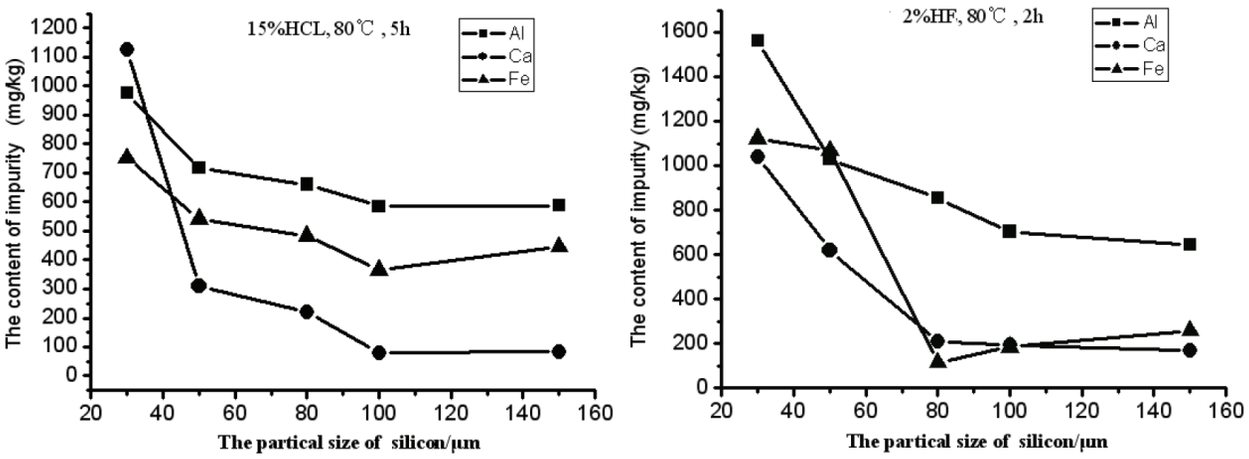

Figure 5. Final impurity content after leaching with hydrochloric acid and hydrofluoric acid at different particle sizes.

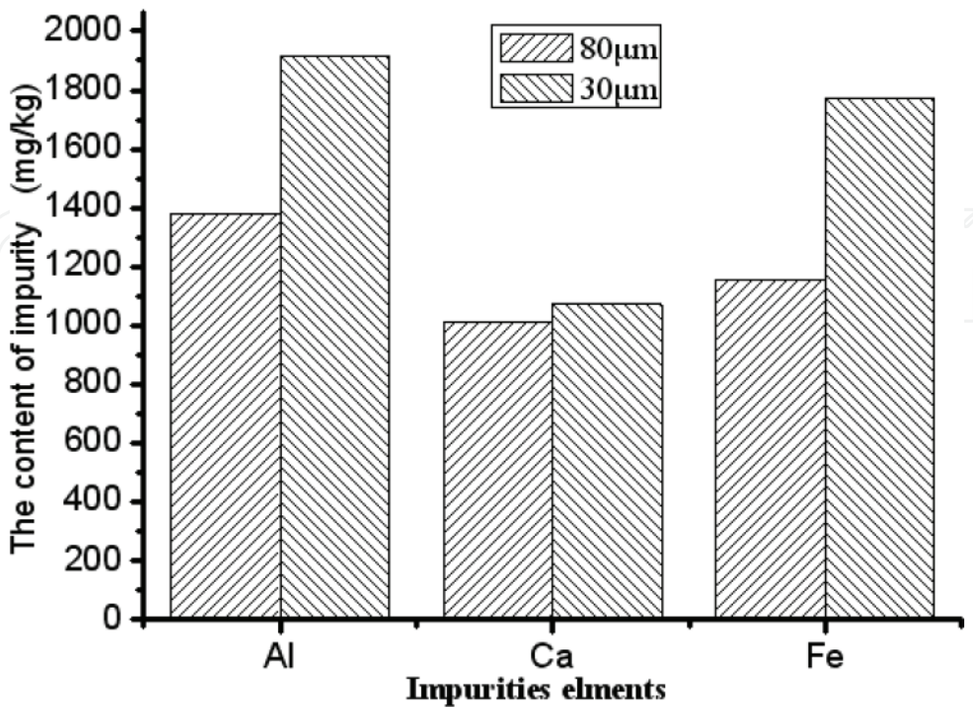

Figure 6. The concentration of major impurities at different particle sizes.

http://dx.doi.org/10.5772/67643

2.2.5. The final purity of silicon at the optimum processing parameters

From the above analysis, the optimum process parameters for acid leaching are as follows: hydrochloric acid, 15%, 80°C, 10 h and 100 μm. The final content of major impurities after leaching with hydrochloric acid and hydrofluoric acid solutions at the optimum processing parameters is represented in **Figure 7**. Although the acid leaching parameters are the optimum processing parameters, final total content of major impurities treated with hydrochloric acid is lower than that treated with hydrofluoric acid. The final purity of silicon powders after leaching with hydrochloric acid and hydrofluoric acid solutions at the optimum processing parameter is denoted in **Figure 8**. The final purity of silicon powders after leaching with hydrochloric acid solution is better than that after leaching with hydrofluoric acid solution, and the final purity of silicon powders after leaching with hydrochloric acid and hydrofluoric acid mixture solutions is a little better than that after leaching with hydrochloric acid alone. Meanwhile, there is no significant differences between silicon treated in one step with mixture acid and treated in two steps, first with hydrochloric acid and then with hydrofluoric acid. When hydrochloric and hydrofluoric acids are used for leaching simultaneously, care must be taken because it might cause explosions under this condition. Hydrogen is generated during acid leaching process and, in addition, because of the presence of silicide (especially calcium and magnesium silicide) in MG-Si, self-igniting silicon hydrides are formed. So adequate safety precaution should be adopted in order to avoid the danger mentioned above and it is better to select hydrochloric acid as the acid leaching solution.

2.3. The acid leaching critical and discussion

From the results obtained till now, the following can be stated: (1) The optimum processing parameters for acid leaching are as follows: hydrochloric acid, 15%, 80°C, 10 h and 100 μm.

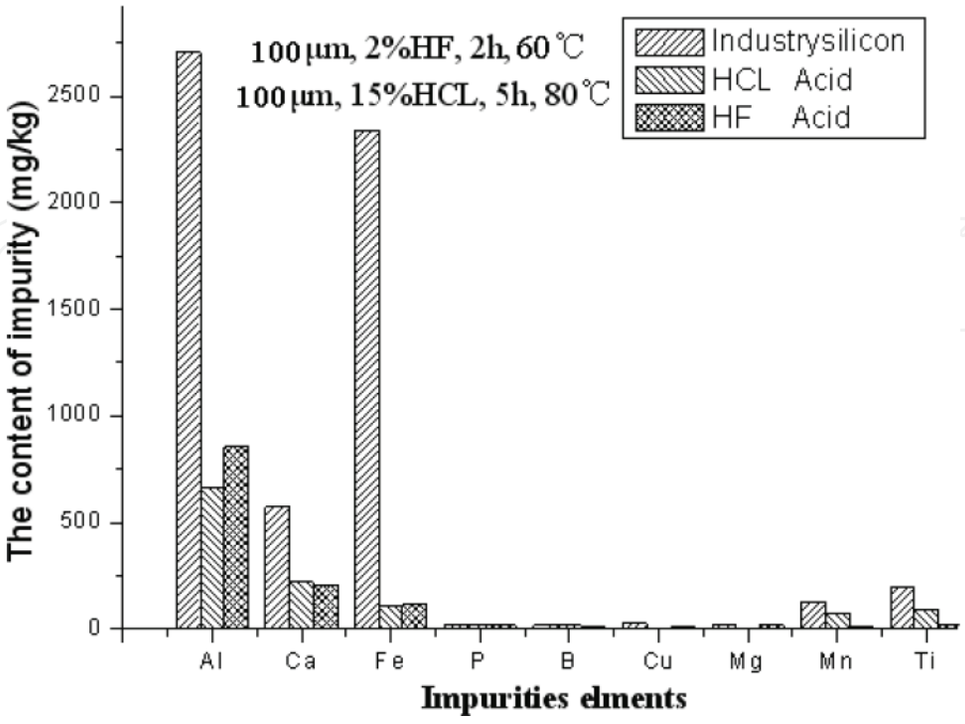

Figure 7. Final content of major impurities after leaching at the optimum process parameters.

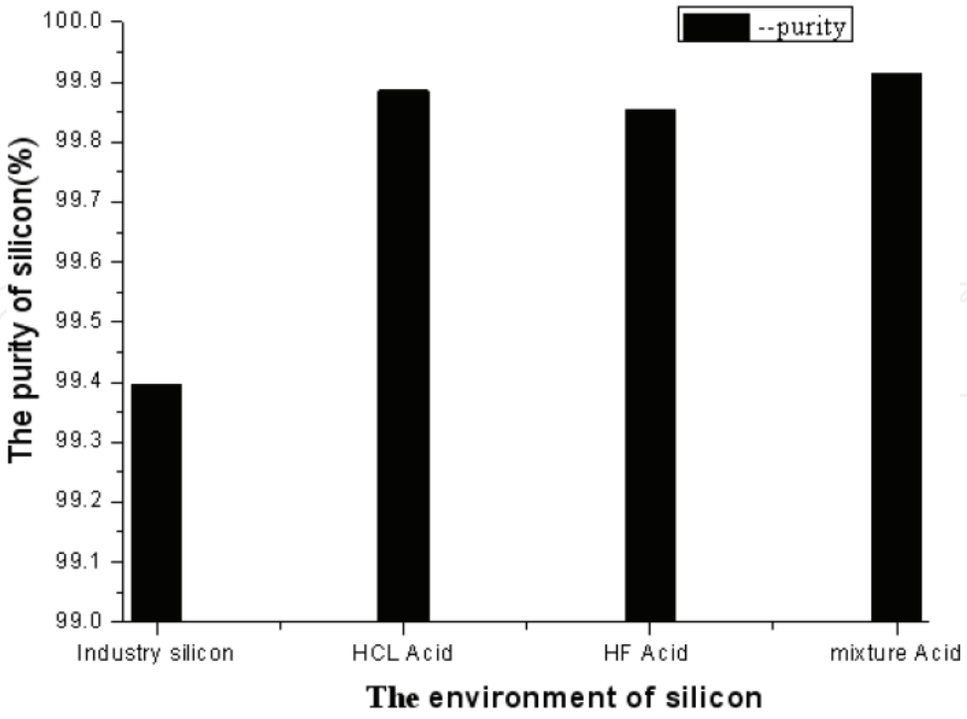

Figure 8. Final purity of silicon powders after leaching at the optimum process parameters.

The removal efficiencies of aluminium, iron and calcium impurities are up to 70.9, 94.82 and 82.69%, respectively. (2) The formation of insoluble fluorides is a rejection for the impurity removal under hydrofluoric acids, and it is dangerous under the mixture of hydrofluoric and hydrochloric acids. In order to avoid the above situation, it is better to select hydrochloric acid as the acid leaching solution. (3) The content of major impurities increases as the particle sizes of MG-Si powders decrease, because the more friable phases contained impurities concentrate in the finer fraction during sieving.

Silicon of 99.9% purity was obtained by leaching with hydrochloric acid alone from MG-Si with iron (0.234%), aluminium (0.271%) and calcium (0.058%) under the optimum process parameters. On the other hand, silicon of above 99.9% purity could be also obtained after leaching with hydrochloric acid and hydrofluoric acid. The significant improvement achieved by mixture solutions was due to the Fe-Si and Fe-Si-Ti phases, which were not leached by hydrochloric acid. Although the silicon powders of 99.9 wt% could be obtained after the acid leaching, the major metallic impurities in MG-Si could not be got rid of fully only with the acid leaching because there was a critical factor in the acid leaching process.

There are two main reasons as follows: the distribution of impurities in MG-Si is non-uniform and their distribution can be divided into two situations: one is light-coloured inclusions, which are confined to the grain boundaries and can be clearly defined at grain boundaries; the other one is dark-colour inclusions, which are distributed clutter-like particles in MG-Si. In order to separate these impurities from MG-Si as much as possible in the wet pre-treatment process, MG-Si needs to be crushed. During the course of this processing, the impurities existed in MG-Si powders by three forms. The first form is a single particle alone in the

http://dx.doi.org/10.5772/67643

MG-Si powders, the second form is partly enchased in the silicon and partly naked to the air, the third form of impurities is completely coated by silicon with no contact with the outside world. When the MG-Si powders are treated with the leaching agent, the first forms of impurity can quickly react with the leaching agent and go into the solution. Leaching rate can be improved through strengthening stir, increasing the leaching agent concentration and reaction temperature and so on. The second form of impurities contacted with the outside world only partially, the reaction between the agent and the impurities needs to keep from outside to inwards, and this reaction is controlled by a chemical reaction process, and leaching rate can be improved by increasing the reaction temperature, the leaching agent concentration and reducing the original particle radius. The third form of impurities in silicon is coated completely without contact with the outside world. Because silicon does not react with the leaching agent and the reaction between the leaching agent and the impurities is difficult, the reaction process is controlled by internal diffusion. Increasing the reaction temperature, reducing the original particle radius and the thickness of solid membrane can improve their leaching rate. Under the wet pre-treatment process, the first forms of impurity can quickly react with the leaching agent and thus they can be removed commendably. The second form of impurities can also be removed after a period of reaction time. The third form of impurities coated in the silicon is difficult to contact and react with the leaching agent as silicon acts as a good barrier coating for impurities [4].

3. Refining of metallurgical grade silicon by electron beam melting

3.1. Research status of silicon purification by electron beam melting

The global PV industry has been rapidly developed over the past 10 years, which led to a large demand for silicon materials. Silicon was divided into four categories according to the purity of itself that is metallurgical grade silicon (MG-Si), chemical grade silicon (CG-Si), solar grade silicon (SOG-Si) and electronic grade silicon (EG-Si). The solar cell is the key technology for the solution of the energy problem in our planet. In order to search a steady material supply for solar cell, a new process to produce silicon with low cost is necessary. A lot of studies had been explored for the production of high purity silicon by EBM processes [5]. The silicon sample with purity of 99.999% was obtained from an initial purity of 99.91% by EBM [6]. Takashi et al. found that 75% aluminium, 89% calcium, 90% carbon and 93% phosphorus were removed by EBM under 10^{-2} Pa and 30 min; in the meantime, first-order rate equation was used for carbon, calcium and aluminium, and second-order equation was fit for the dephosphorization [7]. Kazuhiro et al. [8, 9] carried out industrial scale experiment for EBM purification process. MG-Si with 25 ppmw of phosphorus was successfully purified to below 0.1 ppmw. Osokin V.A. et al. [10] indicated that the phosphorus content decreased from 0.001 to 0.0003% after EBM under a scanning electron beam in an 8.9×10^{-3} Pa vacuum. Silicon ingot with the conversion efficiency of 14.1% was successfully produced by a new technology. The technology includes electron beam, plasma beam and directional solidification prepared SOG-Si, which was invented by Japan's JET Company [11]. Above studies indicated that electron beam melting has been studied in-depth in foreign countries, but it is still at its initial stages in China due to some reasons.

3.2. Impurity removal process and effect analysis of electron beam melting

In order to study preparation of SOG-Si by EBM, in this section, a new technology of purification process that combined EBM and directional solidification would be researched. The content and distribution of impurity at different locations of silicon disk were also discussed by electron probe microanalysis (EPMA). Impurity contents and surface analysis were confirmed by inductively coupled plasma mass spectrometry (ICP-MS) and scanning electronic microscope (SEM). The schematic diagram of structure and principle for EBM is shown in **Figure 9**. Silicon particles were washed with acetone in an ultrasound cleaner with the objective of removing possible solid residues from the surface before EBM and silicon with 0.4 kg was placed in the copper crucible for every time experiment. Silicon material was melted with electron beam until the whole silicon was melted. After refining process, the powder was reduced tardily until the beam disappeared at the centre of the copper crucible, which provides a temperature gradient from outside to inside in the copper crucible. **Table 3** gives the process parameters.

3.2.1. The macro-morphology of silicon disk

Figure 10 shows the top and bottom views of silicon disk obtained after EBM with a diameter of 130 and 25 mm thickness, respectively. The bottom of silicon disk was very coarse because

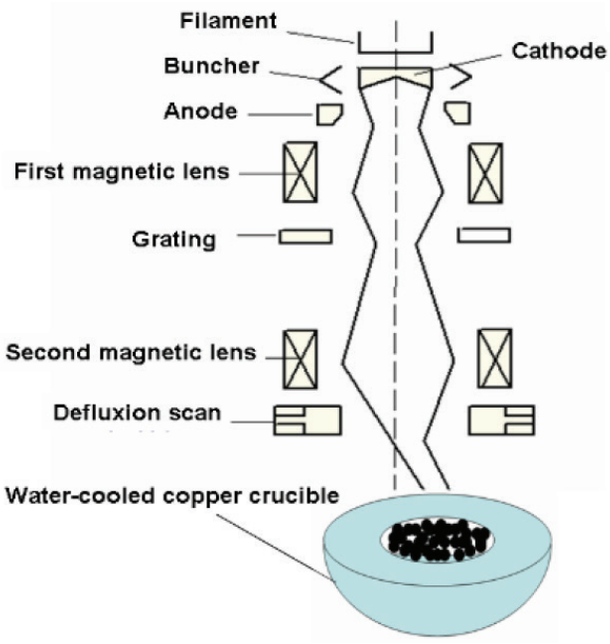

Figure 9. Schematic diagram of structure and principle for electron beam furnace.

Melting time (min)	20
Beam power (kW)	10–15
Internal pressure of the furnace (Pa)	2.5×10^{-3} to 5.0×10^{-3}

Table 3. Experimental parameters used in the electron beam melting.

http://dx.doi.org/10.5772/67643

the bottom of the disk contacted with the refrigerated copper crucible, which led to it not fully melting under EBM.

Figure 11 shows the schematic representation of the regions from silicon disk for impurity profile analysis.

3.2.2. Distribution of impurity elements along axial

Distributions of metal impurity and non-metal elements along axial are shown in **Figures 12** and **13**, respectively. It could be seen that metal impurity was dragged from bottom to top along the direction of solidification. The distribution of non-metal impurity was not affected. The location with the lowest impurity content was at about 10 mm above silicon sample bottom. The metal impurities gathered at the top could be explained by segregation coefficients. Metal impurities were pushed aside the liquid region during solidification process because the effective segregation coefficient of metal impurities in silicon was less than 1. Thus, the content of metal impurities increased gradually along the ingot height direction.

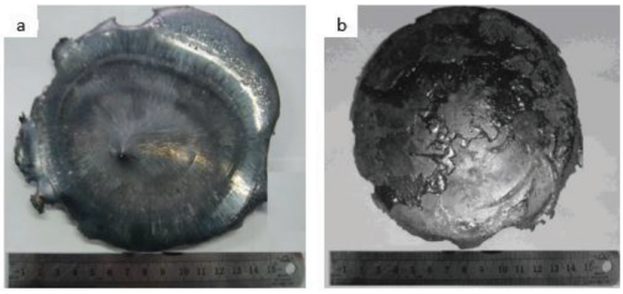

Figure 10. Top view (a) and bottom view (b) of silicon disk after electron beam melting.

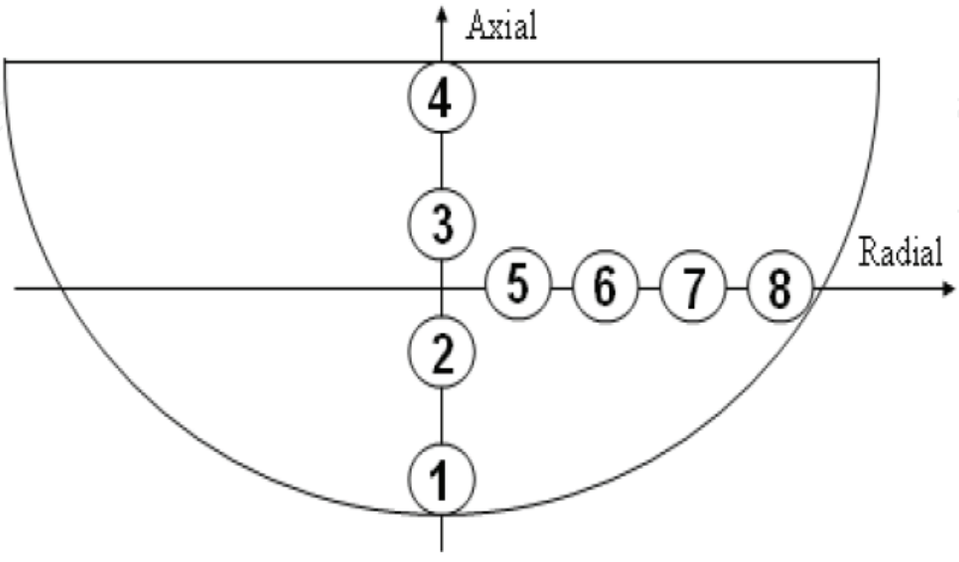

Figure 11. Schematic representation of the regions of silicon disk for impurity profile analysis.

Figure 14 shows the diagram of silicon cake solidification process. There were two temperature gradients during silicon solidification by the special structure of water-cooled copper crucible; they were the axial and the radial temperature gradient. Metal elements were dragged to the remaining liquid region during solidification. Thereby, the solidified part was purified. Elements like Cu, Al, Ti and Fe were segregated effectively to the liquid In the process of solidification because they have low segregation coefficients ($k \ll 1$). However, the non-metal elements like C, O, B and P were little affected because the segregation coefficient of them is close to unit [12]. One noteworthy fact in **Figure 4** is that metal impurities concentrations at the bottom are greater than the area just over it. Non-metallic impurity elements also have the same distribution at the bottom besides B. This could be explained by the fact that the bottom of the silicon disk contacts with the water-cooled copper crucible, so the melting was not sufficient. The bottom of silicon disk has already solidified before metallic impurities had enough time to diffuse fully.

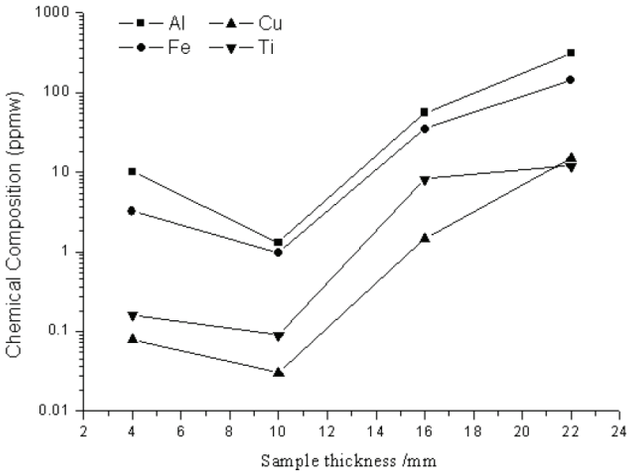

Figure 12. Distribution of metal impurity elements along axial.

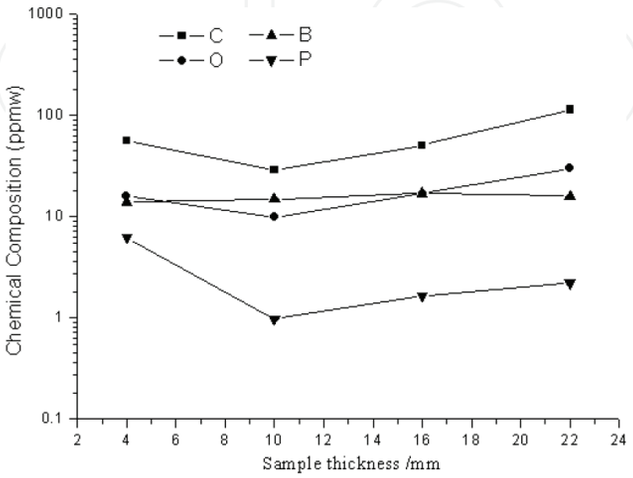

Figure 13. Distribution of non-metal impurity elements along axial.

http://dx.doi.org/10.5772/67643

3.2.3. Distribution of impurity elements along sample radial

Figures 15 and **16** show the distribution of impurity along radial. Metal impurities were also dragged from the edge to the centre in the water-cooled copper crucible. There was almost no change of the non-metal impurities contents from the edge to the centre of the silicon disk. We also found that C element presented the same distribution trends in **Figures 15** and **16**. Carbon could reverse diffusion and could be dragged in the opposite direction of solidification because the segregation coefficient of it was nearer to the unit and the atomic radius of it was also smaller relative to silicon [13]. Silicon carbides precipitation also formed when the carbon concentration was over saturated.

Figure 14. Schematic diagram of the solidification process of silicon cake: (a) the initial stage, (b) the intermediate stage and (c) the end stage.

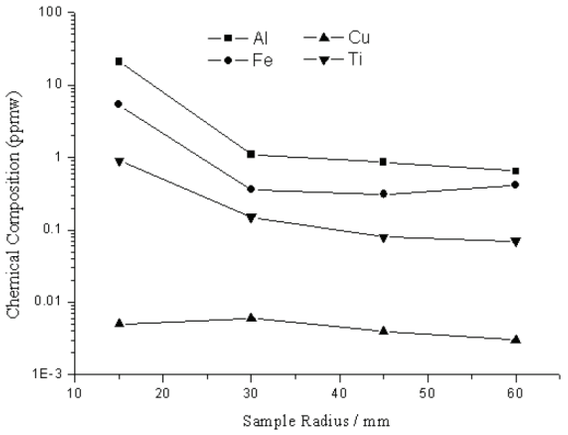

Figure 15. Distribution of metal impurity elements along sample radial.

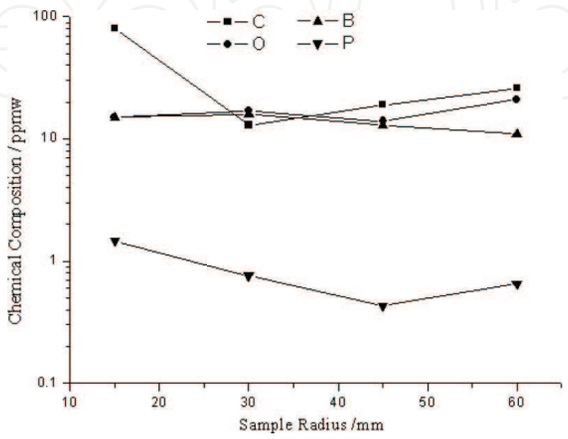

Figure 16. Distribution of non-metal impurity elements along sample radial.

3.2.4. The distribution of impurity elements along axial by electron microprobe analysis

Figure 17(a)–(c) shows the distribution of impurity elements by EPMA corresponding to the metal elements of 4, 2 and 1 sample, respectively.

The distribution of metal elements such as Al, Fe and Ca at the bottom of silicon was very evenly. In the meantime, there was no segregation at the grain boundaries because the bottom of disk contacted the copper crucible, which caused silicon at this position to not fully melt from **Figure 17(c)**. Thus there was no time to spread. From **Figure 17(b)**, it could be seen that metal impurities generated obvious segregation at grain boundaries with the solidification process. At the same time, the number of grain boundaries was very few because the grain size was comparatively large. Most of the inclusions aggregated at the final stage of solidification (the top of solidification portion), due to segregation effects in **Figure 17(a)**. Meanwhile, under the effect of the vertical and horizontal temperature gradient, the grain size decreased and the number of grain boundaries increased. Most of the metal impurities distributed at the grain boundary of silicon crystals owing to the segregation effects and a small number of them was uniformly distributed in grains from the EPMA of the samples. The regularities of distribution for non-metallic elements (such as B and P) were basically the same at the different locations of silicon disk; they scattered equally between grain boundary and grain. The above analysis results were alike along the axial and radial of silicon disk.

3.2.5. Effect of vapour pressure on impurities removal efficiency

Figures 18 and **19** show the changes of metallic and non-metallic impurities in the silicon dealing with different process conditions, respectively. We used sample no. 2 in **Figure 3** to represent the impurity content of silicon cake after electron beam treatment, because the impurities contents in silicon were lowest at this position. From **Figures 18** and **19**, it could be

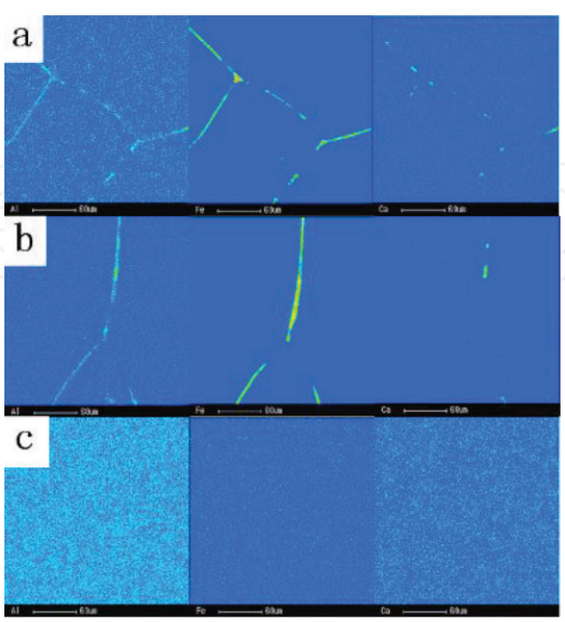

Figure 17. Electron microprobe analysis of metal impurity elements.

http://dx.doi.org/10.5772/67643

seen that metal impurities in silicon had been greatly reduced; however, non-metallic impurities had no change after acid treatment. The contents of metal and non-metallic impurities had been reduced again adequately after EBM. After leaching process, many kinds of impurities elements also remained in MG-Si, but only eight types of impurities still remained in silicon sample after EM because the vapour pressure of Mn, Mg and Ca was higher than that of silicon, therefore, they could be easily removed from silicon by evaporation. The content of Ti, Fe, Al and Cu could also be reduced significantly, although the vapour pressures of them were closer than that of silicon [14]. But the contents of boron did not change along the thickness and radius of silicon after EBM. Because the vapour pressure of this element was very low in relation to that of silicon (10^{-4} Pa of boron and 10^{-1} Pa of silicon) so it was very difficult to remove boron. Therefore, the vacuum process had no effect on its removal. Another reason was the segregation coefficient of boron in silicon was near unit; therefore, unidirectional solidification process for removing boron was also invalid. Plasma melting in an oxidizing atmosphere (O_2, CO_2 or H_2O) for removing boron was effective, boron was transformed into the oxide form (vapour pressure is changed) in this process [15].

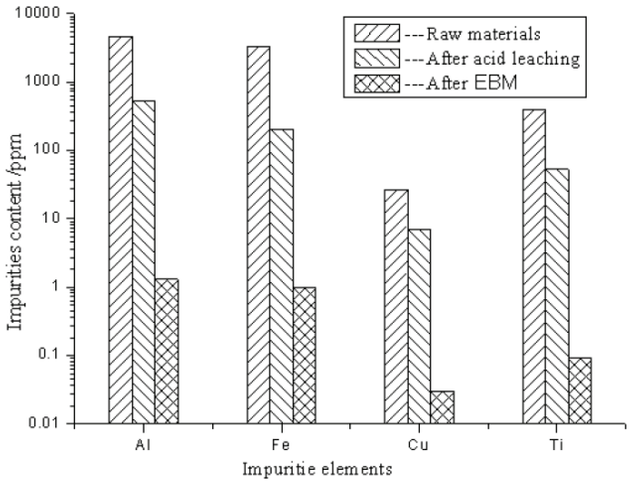

Figure 18. The changes of metal impurities after different treatment processes.

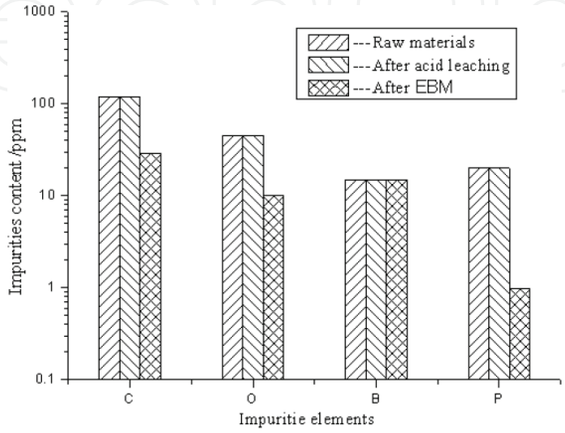

Figure 19. The changes of non-metallic impurities after different treatment processes.

3.3. Limit of impurity removal by electron beam refining

Based on the analysis of the electron beam melting process and the distribution of impurity, we can conclude the following conclusions: (1) Silicon disk (99.995% in mass) was obtained from MG-Si (99.88% in mass) on the centre of the disk after electron beam melting, which had been considered to be a process technically capable of purifying polycrystalline silicon. (2) The distribution characteristics of impurity along sample thickness and sample radius in silicon disk were different. Because metal elements like Cu, Al, Ti, Fe and so on had very low segregation coefficients so they were segregated to the liquid part effectively during solidification. But the non-metal elements like C, O, B, P and so on were a little affected by directional solidification because the segregation coefficient of them was close to unit. (3) The impurities with higher vapour pressure could be removed from silicon easily by evaporation. The impurities like Ti, Fe, Al and Cu with a closer vapour pressure than that of silicon could also be reduced significantly. But it was very difficult to remove the boron because its vapour pressure was very low in relation to the vapour pressure of silicon (10^{-4} Pa for boron and 10^{-1} Pa for silicon) and its segregation coefficient in silicon was near unit.

4. Removal of boron from metallurgical grade silicon (MG-Si) by electromagnetic induction slag melting

4.1. Characteristics and their removal methods of boron impurities in silicon

Scrap of SEG-Si is the main supply for solar cells, but it is difficult to afford a steady supply. Therefore, alternative production processes are needed, refining of metallurgical grade silicon is a very feasible process [16]; however, removing boron by vacuum processes is very difficult because the vapour pressure of boron is very low in relation to that of silicon (10^{-4} Pa for boron and 10^{-1} Pa for silicon). Another difficulty regarding boron extraction is that its segregation coefficient in silicon is near unit which results that there is no removal effect by unidirectional solidification process difficult [17]. A process usually used for the boron removal is plasma melting in an oxidizing atmosphere (O_2, CO_2 or H_2O). In this process, boron is transformed into the oxide form, increasing its vapour pressure [18, 19]. However, it needs a very large initial investment using plasma equipment. Slag refining is very effective method for the removal of boron from molten silicon. The technical viability of the slag refining process has been demonstrated by many researches, but all of them were based on laboratory scale, static theoretical research. Meanwhile, refining time was very long in their study. The values of L_B obtained from their experiments were mostly between 1.5 and 2.5 [20–24]. Meantime, the partition ratio of boron between SiO_2-CaO-Na_2O and SiO_2-CaO-Al_2O_3 slag systems and liquid Si melt at 1823 K were also simulated using the new assessed thermochemical databank together with the FACT oxide thermodynamic database by Bale et al. [25]. The calculated values were approximately two times higher than the experimental values, which indicated that the reaction kinetic barriers might play important roles in

http://dx.doi.org/10.5772/67643

the refining processes. In the present study, pilot scale and dynamic slag experiments were carried out by using electromagnetic induction slag melting. The partition ratio L_B, which is the ratio of the content of impurities in the slag to the content of silicon, has been measured, and the removal effects of some metallic impurities are also analysed. The mechanism of boron by EISM was discussed. Additionally, the thermodynamics and kinetics of boron removal were also carried out. Microanalysis and impurity contents were analysed by inductively coupled plasma atomic emission spectrometer (ICP-AES) and electron probe microanalysis (EPMA).

4.2. Experiment results and analysis of electromagnetic induction slag

4.2.1. The testing process and parameters of electromagnetic induction slagging

The schematic diagram of experimental devices is shown in **Figure 20**. An inductive furnace with 200 kW and 3000 Hz was used for melting. The silicon was loaded in a quartz ceramic crucible with an inner diameter of 120 mm and height of 220 mm. The crucible was surrounded by a graphite heater since because at room temperature it was not a conductor. The induction melting of silicon was carried out through water-cooled copper coil under protective gas. Three kinds of slag systems were chosen according to previous studies and the CaO/SiO_2 ratios in all slag systems was 1.21. Silicon material has already been treated by acid leaching, metal impurities have been reduced significantly but non-metallic impurities such as B and P did not change. In each experiment, 3 kg silicon and 0.3 kg slag (10 wt% of silicon) were used. The boron and metal impurities contents in the silicon phase and the slag phase were analysed by ICP-AES. The partition ratio of boron was defined as follows:

$$L_B = \frac{(\text{ppm\% B})}{[\text{ppm\% B}]} \tag{1}$$

where (ppm% B) and [ppm% B] are the concentrations of boron in slag and silicon, respectively. Experimental conditions and parameters were shown in **Table 4**.

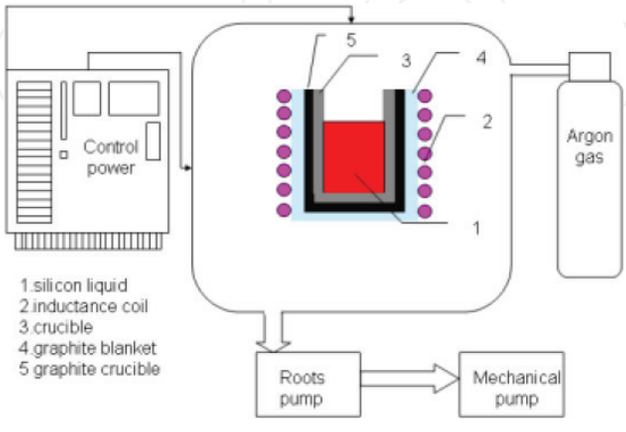

Figure 20. The schematic diagram of experimental devices.

4.2.2. The test parameters of electromagnetic induction on slagging boron removal effect

4.2.2.1. The effect of the third oxide and refining time on boron removal

Four types of typical slag systems were chosen for comparative study according to the previous research [20–23]. The photograph of silicon ingots after test is shown in **Figure 21**. From **Figure 21(a)**, it could be found that the most slag froze at the bottom of silicon ingots after test and a small amount of them covered at the side of silicon ingot. Slag deposited to the bottom of the crucible and solidified here because the density of slag and silicon melt is different, the former is larger. So, they can be well separated. The internal silicon ingot was very bright, and no slag agent in the inner was found from **Figure 21(b)**. This proved again that the slag and silicon could separate very well.

The values of L_B after melting test under different types of slag at 1773 K for 1 h are shown in **Figure 22**. It could be seen that boron removal was significantly improved by using EISM compared to previous static test results [19–21]. Although CaO/SiO_2 ratios were same in different slag systems, the values of L_B were very different by adding different third oxide to the CaO/SiO_2 slag system. The values of L_B significantly reduced by adding CaF_2 but significantly enhanced by adding Na_2O and Al_2O_3. Therefore, this chapter focused on the removal of boron at different refining parameters under SiO_2-CaO-Na_2O and SiO_2-CaO-Al_2O_3 slag systems. The reasons for above phenomenon would be presented in the thermodynamic analysis section of this article.

Parameters	Conditions
Initial boron content in silicon	15 ppm
Sorts of used slags	SiO_2-CaO; SiO_2-CaO-(10 wt%)CaF_2
SiO_2-CaO-(10 wt%)Na_2O; SiO_2-CaO-(10 wt%)Al_2O_3	Experimental times
0.5–2 h	Experimental temperatures
1723–1873 K	Atmosphere
High purity Ar(99.999%)	

Table 4. Experimental conditions in the slag treatment.

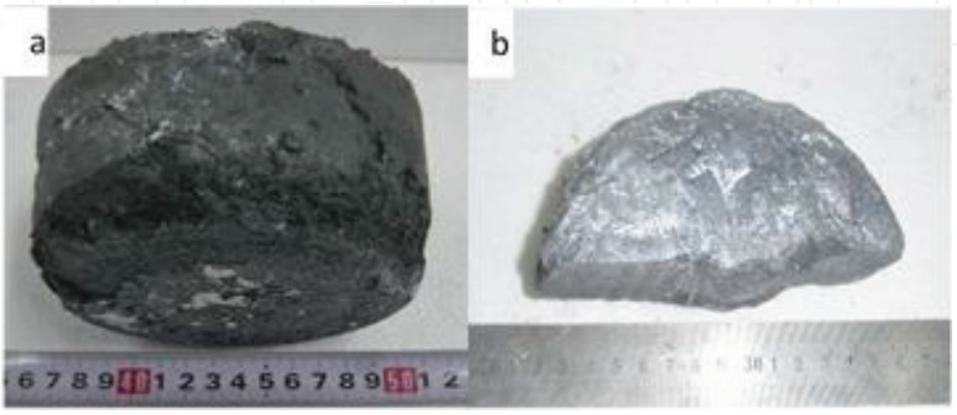

Figure 21. Photos of silicon ingot after electromagnetic induction slag melting.

http://dx.doi.org/10.5772/67643

Figure 23 shows the change of boron removal with refining time at 1823 K under SiO_2-CaO-Na_2O and SiO_2-CaO-Al_2O_3 slag systems. It could be found that L_B was significantly improved compared to previous studies (L_B value was in the range1.5–2.5) by EISM though change situation of L_B in the two kinds of slag systems was different. Diffusion resistance of impurity elements at the boundary layer could be reduced and the diffusion of them also enhanced by increasing the melt flow rate under EISM. So the removal rate of boron could be greatly sped up and the required refining time was also reduced substantially. Impurity removal effect was obviously better under SiO_2-CaO-Al_2O_3 slag systems than that under SiO_2-CaO-Na_2O systems. And L_B value gradually increased with the increasing times under the SiO_2-CaO-Al_2O_3 systems. This showed that the increase in refining time was conducive to the removal of boron. But L_B value increased and then reduced with the increasing times because the use of Na_2O might increase the basicity and also decrease the melting point of the slag. However, sodium oxide could be easily reduced to the silicon phase and became volatile at high temperatures, which made it difficult to work for a prolonged period [22].

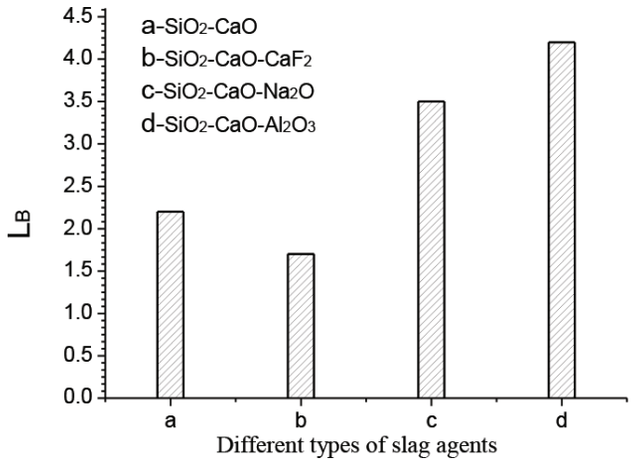

Figure 22. Partition ratio L_B under different types of slag systems.

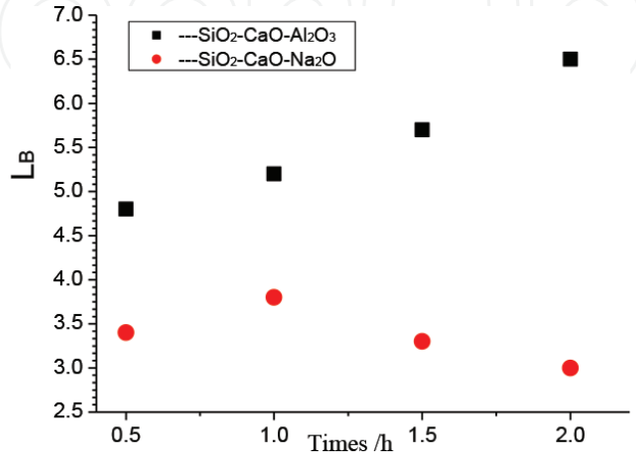

Figure 23. Partition ratio L_B at different times at 1823 K.

4.2.2.2. The effect of refining temperature and slag composition on boron removal

Figure 24 shows the change of boron removal with refining temperatures for 1 h under SiO_2-CaO-Na_2O and SiO_2-CaO-Al_2O_3 slag systems. The value of L_B gradually increased with the increase of refining temperatures under SiO_2-CaO-Al_2O_3 slag systems. The removal effect of boron was raised along the refining temperatures and is increased owing to the viscosity of slag agent debased along with the temperature increased. at the same time, the silica activity in slag and the mobility of slag both enhanced. The above conditions were both conducive to the removal of boron. However, under the SiO_2-CaO-Na_2O systems the removal effect of boron was better at low temperatures than that at high temperatures. The reason for it was also because sodium oxide could be easily reduced to the silicon phase and became volatile at high temperatures [22].

Figure 25 shows the changes of boron removal with the content of Na_2O and Al_2O_3 in slag. L_B had the same change trend with the content of Na_2O and Al_2O_3 in SiO_2-CaO-Na_2O and SiO_2-CaO-Al_2O_3 slag systems. It increased as the proportion of Na_2O and Al_2O_3 in slag increased. The better partition ratio and a higher value for capacity could be obtained if compounds with higher basicity than that of CaO or CaF_2 were selected because both the basicity of slags and the activity of silica in slag could be greatly improved by adding alkaline oxide into slag [22].

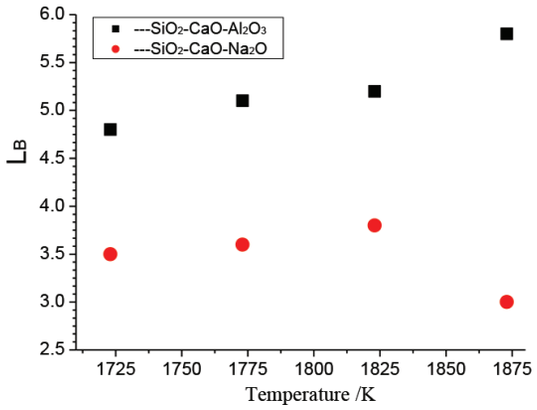

Figure 24. Partition ratio L_B at different temperatures for 1 h.

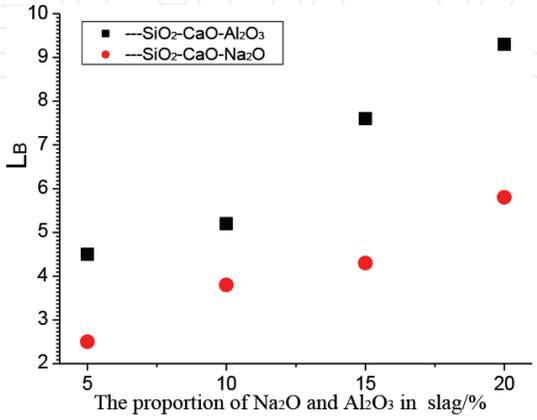

Figure 25. Partition ratio L_B with different contents of Na_2O and Al_2O_3 in slag at 1823 K for 1 h.

http://dx.doi.org/10.5772/67643

4.2.2.3. Removal of other impurity elements

Not only the boron elements could be easily removed by EISM but also other elements could be removed such as Ca, Al and Mg. **Figure 26** shows that Al, Ca and Mg elements could be removed by slag refining; meanwhile their removal rates were 85.0, 50.2 and 66.7%, respectively. **Figure 27** shows the analysis of metal impurity in silicon and slag by EPMA after refining for 2 h at 1823 K under SiO_2-CaO-Al_2O_3 systems. It could be clearly seen that the distribution of Ca, Al and Mg elements was same on both sides of the interface between silicon and slag. They all concentrated in slag phase. The Ca and Al in the slag did not contaminate silicon melt because the state of them existed in slag was relatively stable and the form of them contacted with silicon liquid was molten oxide. Therefore silicon liquid could not be contaminated. Al and Mg elements were more inclined to gather at slag phase because the oxygen content in slag phase was relatively high and the affinity of these two elements with slag was greater than that of silicon.

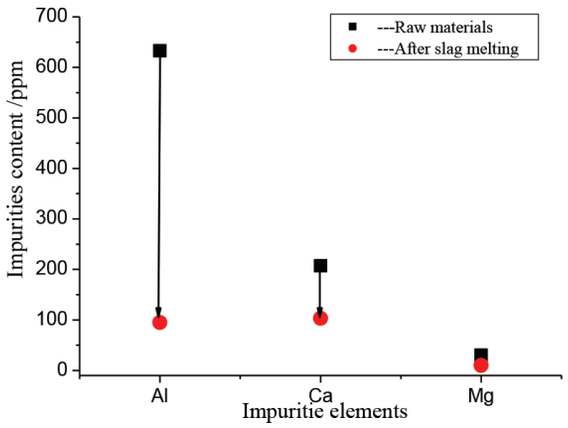

Figure 26. Impurity elements content of silicon before and after slag refining at 1823 K for 2 h.

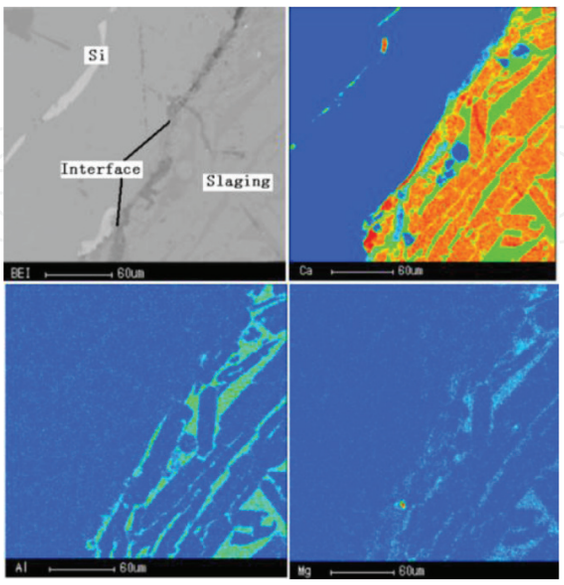

Figure 27. EPMA of metal impurity elements in silicon and slag after refining at 1823 K for 2 h.

4.3. Thermodynamic and Kinetic analysis of boron removal

4.3.1. Thermodynamic analysis of boron removal

The reaction of removal of boron from Si by using basic fluxes could be expressed by Eq. (2):

$$\underline{\mathrm{B}} + \frac{3}{4}(\mathrm{SiO_2}) = \frac{3}{4}\,\mathrm{Si} + (\mathrm{BO_{1.5}}) \tag{2}$$

The boron dissolved from silicon liquid to the slag at the interface and silica got reduced and entered the liquid melt, boron element got oxidized and entered the slag due to chemical reaction. The distribution coefficient of boron was given as the ratio by Eq. (3):

$$L_{\mathrm{B}} = \frac{(\%\,\mathrm{B})}{[\%\,\mathrm{B}]} = \frac{K f_{\mathrm{B}}}{\gamma_{\mathrm{BO_{1.5}}} k_{x\to\%}} \left(\frac{a_{\mathrm{SiO_2}}}{a_{\mathrm{Si}}}\right)^{3/4} \tag{3}$$

where the square brackets denote boron dissolved in the silicon and parentheses denote boron in the slag. From **Figure 3**, it could be known that removal effect of boron under SiO_2-CaO-Na_2O and SiO_2-CaO-Al_2O_3 slag systems was better than that under SiO_2-CaO-CaF_2. The reason was as follows: the activity coefficient of boron oxide was calculated for CaO/SiO_2-based slag at 1723–1873 K and could be approximately expressed as Eq. (4):

$$\ln \gamma_{\mathrm{BO_{1.5}}} = -4.00\left(\mathrm{CaO/SiO_2}\right) + 3.67 \tag{4}$$

When CaF_2 was added in the slag, CaO could be generated after CaF_2 reacted with silica, thereby increasing the basicity of slags. Although the addition of CaF_2 provided a broader basicity range compared to the binary system, the content of SiO_2 in slag reduced and the oxygen partial pressure also significantly reduced. Meanwhile, the ratio of CaO/SiO_2 in Eq. (4) increased and resulted $\gamma_{\mathrm{BO_{1.5}}}$ also reduced. But the change degree $\gamma_{\mathrm{BO_{1.5}}}$ was small relative to $(a_{\mathrm{SiO_2}}/a_{\mathrm{Si}})^{3/4}$. Therefore, L_{B} would reduce according to Eq. (3) [23]. It was apparent that when Na_2O and Al_2O_3 were added in slag, a better partition ratio and a higher value for capacity might be obtained. This was because not only the basicity of slag could be greatly improved but also the oxygen partial pressure of slag could also be greatly increased by adding alkaline oxide into slag. In this case, the oxygen partial pressure of $(a_{\mathrm{SiO_2}}/a_{\mathrm{Si}})^{3/4}$ also significantly increased. Meanwhile, the ratio of CaO/SiO_2 in Eq. (4) increased and resulted $\gamma_{\mathrm{BO_{1.5}}}$ also reduced. So L_{B} would increase according to Eq. (3). In addition, the use of Al_2O_3 might decrease the melting point of the slag and the mobility and affinity of slag were also improved markedly [24]. L_{B} value gradually increased with temperatures under EISM. This was because the activity coefficient of boron $\left(f_{\mathrm{B}}^{0}\right)$ in dilute solution silicon was expressed by Eq. (5) between 1723 and 1923 K [22]:

$$\log f_{\mathrm{B}}^{0} = -\frac{1.11\times10^{4}}{T} + 5.82 \tag{5}$$

increased with temperature. Meanwhile, the equilibrium constant K also increased. The effect of temperature on $\gamma_{\mathrm{BO_{1.5}}}$ was very small, so it could be ignored. The activity coefficient of boron oxide was affected by the incorporation between boron and silicate network. The further decreased on $\gamma_{\mathrm{BO_{1.5}}}$ as the silica content increased was not necessarily a function of the amount of boron incorporated in the network but might be related to the degree of polymerization of the slag structure. So, L_{B} would increase according to Eq. (3) under SiO_2-CaO-Al_2O_3 slag system. But L_{B} value would reduce with the increasing temperatures under the SiO_2-CaO-Na_2O slag system because Na_2O could easily become volatile at high temperatures [22]. Because

http://dx.doi.org/10.5772/67643

the boron was micro in the silicon, boron diffuson from silicon into slag phase needed certain time. This will be discussed in detail in the following section.

4.3.2. Kinetic analysis of boron removal

Following five steps were needed in refining impurity element by slag refining: (1) impurity transfers from the bulk metallic phase to the metal boundary layer $[\%X]_b \rightarrow [\%X]_\delta$; (2) impurity diffuses through the metal boundary layer $[\%X]_\delta \rightarrow [\%X]_i$; (3) metal impurity was oxidized at the interface between metal melt and slag melt $[\%X]_i \rightarrow (\%X)_i$; (4) impurity spread through the slag boundary layer $(\%X)_i \rightarrow (\%X)_\delta$ and (5) impurity transferred from the slag boundary layer to slag bulk phase $(\%X)_\delta \rightarrow (\%X)_b$. Above process depended on stirring and mixing between silicon fluid and slag. We often use gas bubbling or mechanical devices to increase the mass transfer in the bulk phases. Therefore, the viscosity of slag properties was important. The low velocities in the slag and the low mass transfer of the impurity element could be obtained if the slag had a high viscosity; meanwhile, the diffusivity of the impurity element was also lowered. The mass transfer coefficients β (in the metal) and β_S (in the slag) determined processes for Steps 2 and 4, respectively. A serious difficulty with refining silicon by extraction to a second (slag) phase was the problem of mixing in the slag phase. Often, the slag phase was relatively viscous, so that it was difficult to mix the impurity element throughout the slag.

In this section, we used the electromagnetic induction slag refining method. The melt movement which was produced by electromagnetic force in the crucible is shown in **Figure 28**. Electromagnetic force was formed due to the interaction function by the induction eddy current in melt and the magnetic field in the medium frequency induction coil. Slag agent followed the silicon fluid movement and they could contact fully in crucible because the electrical conductivity of them was different. Electromagnetic induction melting was better relative to gas mixing and mechanical agitation because Electromagnetic induction melting process did not contact with silicone melt and did not lead into other impurities. The effective boundary layer thickness (units) is as follows according to boundary layer theory:

$$\delta = \frac{c - c^*}{\left(\frac{\partial c}{\partial x}\right)_{x=0}} \tag{6}$$

where c^* is the concentration for interface and c is the concentration for liquid bulk concentration outside the boundary layer ($c^* > c$). In addition, the mass transfer coefficient of impurity could be expressed as follows by the surface renewal theory:

$$\beta = \sqrt{DS} \tag{7}$$

where D is the diffusion coefficient for impurity element and S is the surface renewal rate.

The boundary layer thickness was thinner as the concentration gradient near interface was larger by Eq. (6). Thickness of boundary layer could be reduced if the concentration gradient became larger by increasing fluid flow. Diffusion resistance did not exist finally when the flow rate increased (run up to critical velocity) until the thickness of boundary layer achieved zero. Diffusion resistance of impurity elements at the boundary layer could be reduced and the diffusion of them could be enhanced with the increase in the melt flow rate by electromag-

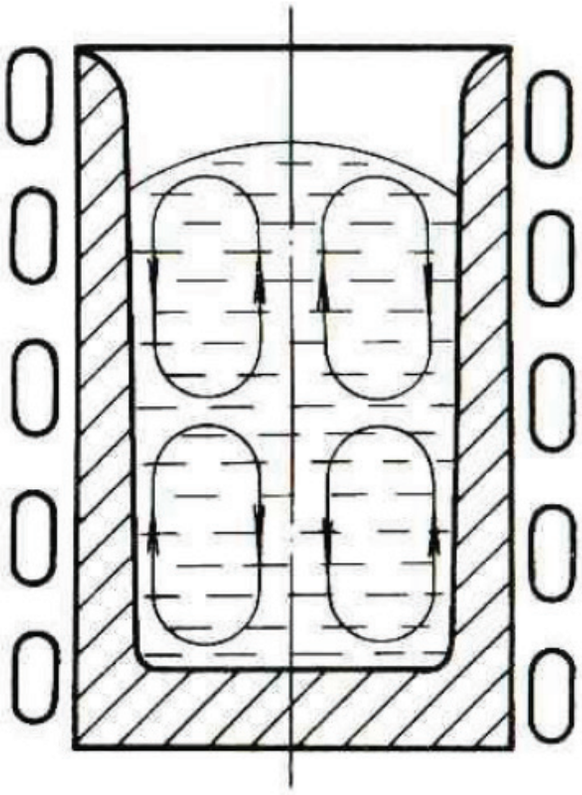

Figure 28. The flow lines of silicon melt under electromagnetic induction melting.

netic stirring. At the same time, the diffusion coefficient of impurity elements also could be enhanced. The mass transfer coefficient β and β_S both had been increased according to Eq. (7). Therefore, the removal of boron could be improved and sped up.

The above is why the boron impurities in silicon could be significantly reduced by the EISM.

4.3.3. Conclusion

The following conclusions can be drawn from the above experimental process and analysis process: (1) MG-Si with 15 ppm of boron was successfully purified to 2 ppm after EISM at 1823 K for 2 h under SiO_2-CaO-Al_2O_3 slag systems. Meanwhile, Al, Ca and Mg elements in MG-Si were also well removed and their removal efficiency reached 96.4, 91.8 and 76.2%, respectively. (2) The value of L_B increased with temperature and refining time owing to the mobility of slag is enhanced and the viscosity of slag agent is reduced; meanwhile, the silica activity in slag increases along with increase in temperature. (3) The boron content of silicon could be significantly improved and the level of it achieved the SOG-Si requirement after EISM because diffusion resistance of impurity at the boundary layer could be reduced and the diffusion of impurity could be enhanced by increasing the melt flow rate. At the same time, the mass transfer coefficient β and β_S both had been enhanced; therefore, the removal of boron could be improved and sped up. Above discussion showed that EISM was a very effective method for removal of boron from silicon.

Acknowledgements

This research was supported by the National Natural Science Foundation of China (No. 50674018); young- and middle-aged backbone teachers training program of Chengdu University of Technology (No. 10912-JXGG201516) and Key Natural Science Foundation of Sichuan Provincial Department of Education (No. 15ZA0079).

Author details

Dawei Luo

Address all correspondence to: luodawei2013@cdut.cn

College of Materials, Chemistry & Chemical Engineering, Chengdu University of Technology, Sichuan, China

Collaborative Innovation Centre of Panxi Strategic Mineral Resources Multi-Purpose Utilization, Chengdu University of Technology, Chengdu, Sichuan, China

References

[1] Dietl J. Hydrometallurgical purification of metallurgical grade silicon. Solar Cells, 1983, 10:145–154. DOI:10.1007/s12598-009-0043-1.

[2] Kantos I.C., Gonalves A.P., Santos C.S., et al. Purification of metallurgical grade silicon by acid leaching. Hydrometallurgy, 1990, 23(2–3): 237–246. DOI:10.1016/0304-386X(90)90007-O.

[3] Kotval P.S. Process for the production of refined metallurgical silicon, U.S. Patent 4195067, 1997. ID: lens.org/125-322-381-086-850.

[4] Zhan L.Y. Pre-treatment experimental study of direct preparation solar grade silicon from metallurgical grade silicon [thesis]. Kunming University of Science and Technology, Kunming, 2007.

[5] Maijer D.M., Ikeda T., Cockcroft S.L., Maeda M., Rogge R.B. Mathematical modelling of residual stress formation in electron beam remitting and refining of scrap silicon for the production of solar-grade silicon. Materials Science and Engineering, 2005, 390:188–201. DOI:10.1016/j.msea.2004.08.036.

[6] Pires J.C.S., Braga A.F.B., Mei P.R. Profile of impurities in polycrystalline silicon samples purified in an electron beam melting furnace. Solar Energy Materials and Solar Cells, 2003, 79:347–355. DOI:10.1016/S0927-0248(02)00471-3.

[7] Takashi I., Masafumi M. Purification of metallurgical silicon for solar grade silicon by electron beam button melting. Iron and Steel Institute of Japan International, 1992, 32:635–642. DOI:10.2355/isijinternational.32.635.

[8] Kazuhiro H., Noriyoshi Y., Yoshiei K. Evaporation of phosphorus in molten silicon by an electron beam irradiation method. Materials Transactions, 2004, 45:844–849. DOI:10.2320/matertrans.45.844.

[9] Noriyoshi Y., Kazuhiro H., Yoshiei K. Removal of metal impurities in molten silicon by directional solidification with electron beam heating, materials transactions, 2004, 45:850–857. DOI:10.2320/matertrans.45.850.

[10] Osokin V.A., Shpak P.A., Ishchenko V.V., Panibratskii V.A., Piyuk E.L. Electron-beam technology for refining polycrystalline silicon to be used in solar power applications. Metallurgist, 2008, 52:121–127. DOI:10.1007/s11015-008-9018-y.

[11] Yuge N., Abe M., Hanazawa K., Baba H., Nakamura N., Kato Y., Sakaguchi Y., Hiwasa S., Aratani F. Purification of metallurgical grade silicon up to solar grade. Progress in Photovoltaics: Research and Applications, 2001, 9:203–209. DOI:10.1002/pip.372.

[12] Möller H.J. Semiconductors for solar cell applications. Progress in Materials Science, 1991, 35:205–206. DOI:10.1016/0079-6425(91)90001-A.

[13] Barbosa L.C., Zone refining of silicon. [thesis], Faculdade de Engenharia de Campinas, Universidad Estadual de Campinas, Campinas, São Paulo, Brazil, 1981.

[14] Pires J.C.S., Otubo J., Braga A.F.B., Mei P.R. The purification of metallurgical grade silicon by electron beam melting. Journal of Materials Processing Technology, 2005, 169:16–20. DOI:10.1016/j.jmatprotec.2004.03.035.

[15] Ikeda T., Maeda M. Elimination of boron in molten silicon by reactive rotating plasma arc melting. Materials Transactions Japan Institute of Metals, 1996, 37:983–987. DOI:10.2320/matertrans1989.37.983.

[16] Braga A.F.B., Moreira S.P., Zampieri P.R., Bacchin J.M.G. Mei P.R. New processes for the production of solar-grade polycrystalline silicon: A review. Solar Energy Materials & Solar Cells, 2008, 92:418–424. DOI:10.1016/j.solmat.2007.10.003.

[17] Ciszek T.F., Schwuttke G.H., Yang K.H. Solar-grade silicon by directional solidification in carbon crucibles. IBM journal Of research Develop, 1979, 23:270–277. DOI:10.1147/rd.233.0270.

[18] Takashi I., Masafumi M. Elimination of boron in molten silicon by reactive rotating plasma arc melting. Materials Transactions Japan Institute of Metals, 1996, 37:983–987. DOI:10.2320/matertrans1989.37.983.

[19] Wu J.-J., Ma W.-H., Yang B., Dai Y.-N., Morita K. Boron removal from metallurgical grade silicon by oxidizing refining. Transactions of Nonferrous Metals Society of China, 2009, 19: 463–467. DOI:10.1016/S1003-6326(08)60296-4.

[20] Liaw H.M., Secco F. Purification of metallurgical grade silicon by slagging and impurity redistribution. Solar Cells, 1983, 10:109–118. DOI:10.1016/0379-6787(83)90012-1.

[21] Ryouji N., Kichiya S., Fumitaka T., Nobuo S. Thermodynamics of boron in silicon melt. Metallurgical and materials transactions B, 1994, 25:903–907. DOI:10.1007/BF02662772.

[22] Torsten W., Klaus S. Chemical equilibria between silicon and slag melt. Metallurgical and Materials Transactions B, 1994, 25:497–504. DOI:10.1007/BF02650071.

[23] Leandro A., Viana T., Kazuki M. Removal of boron from molten silicon using CaO-SiO_2 based slags. Iron and Steel Institute of Japan International, 2009, 49:783–787. DOI:10.2355/isijinternational.49.783.

[24] Leandro A., Viana T., Yomei T., Toshinobu Y., Kazuki M. Behavior and state of boron in CaO-SiO_2 slags during refining of solar grade silicon. Iron and Steel Institute of Japan International, 2009, 49:777–782. DOI:10.2355/isijinternational.49.777.

[25] Bale C.W., Chartrand P., Degterov S.A., Eriksson G., Hack K., Mahfoud R.B., Melançon J., Pelton A.D., Petersen S. FactSage thermochemical software and databases, Calphad, 2002, 26:189–228. DOI:10.1016/j.calphad.2008.09.009.

IntechOpen